



OPEN Immobilized *Saccharomyces cerevisiae* viable cells for electrochemical biosensing of Cu(II)

Ehtisham Wahid^{1,6}, Ohiemi Benjamin Ocheja^{2,6}, Sunday Olakunle Oguntomi³, Run Pan³, Matteo Grattieri^{4,5}, Nicoletta Guaragnella², Cataldo Guaragnella¹ & Enrico Marsili³✉

Electrodes functionalised with weak electroactive microorganisms offer a viable alternative to conventional chemical sensors for detecting priority pollutants in bioremediation processes. Biofilm-based biosensors have been proposed for this purpose. However, biofilm formation and maturation require 24–48 h, and the microstructure and coverage of the electrode surface cannot be controlled, leading to poorly reproducible signal and sensitivity. Alternatively, semiconductive biocompatible coatings can be used for viable cell immobilization, achieving reproducible coverage and resulting in a stable biosensor response. In this work, we use a polydopamine (PDA)-based coating to immobilize *Saccharomyces cerevisiae* yeast viable cells on carbon screen printed electrodes (SPE) for Cu(II) detection, with potassium ferricyanide ($K_3[Fe(CN)_6]$) as a redox mediator. Under these conditions, the current output correlates with Cu(II) concentration, reaching a limit of detection of 2.2 μ M, as calculated from the chronoamperometric response. The bioelectrochemical results are supported by standard viability assays, microscopy, and electrochemical impedance spectroscopy. The PDA coatings can be functionalised with different mutant strains, thus expanding the toolbox for biosensor design in bioremediation.

Keywords Polydopamine, Biosensors, Bioremediation, *Saccharomyces cerevisiae*, Extracellular electron transfer

Since Leland Clark Jr developed the amperometric glucose electrode in 1962, electrochemical biosensors have found extensive use in clinical, environmental, industrial, and agricultural applications¹. These biosensors integrate bioreporters (such as viable cells, aptamers, DNA, peptides, antigens) with electrochemical transducers (electrodes or field-effect transducers), making them suitable for miniaturization, batch fabrication, and integration with electronic systems. Moreover, the signal collection devices are cost-effective, portable, and energy-efficient, which is crucial for point-of-care diagnostics^{2–4}. Despite these advantages, few electrochemical biosensors have reached the industrial stage, mainly due to the lack of affinity recognition between bioreporters and analytes. In addition to bacteria, unicellular yeasts have gained attention as bioreporters due to their robustness and ease of modification^{5–8}. *S. cerevisiae* is particularly promising as it is tolerant to extreme environments, genetically tractable, and non-pathogenic⁹. *S. cerevisiae* can utilize both fermentable and non-fermentable carbon sources for energy production¹⁰, and it can also produce electrical signals while oxidizing organic compounds^{9,11,12}. However, the low efficiency of extracellular electron transfer (EET) and the cumbersome process of cell immobilization still limit its practical applications^{13,14}. Recently, the encapsulation of viable cells using PDA has been proposed to protect electroactive biofilms from acid shock¹⁵. PDA, a biopolymer derived from mussel adhesive proteins¹⁶, undergoes self-polymerization in alkaline conditions, forming strong covalent bonds with cell wall proteins, facilitating EET, and improving biocompatibility and stability^{15–19}. Yeast cells in PDA coatings show potential for various applications, including biocatalytic asymmetric reduction and cytoprotection^{20,21}. *S. cerevisiae* yeast cells, which display metabolic inhibition in the presence of metal pollutants, can be immobilized in PDA coatings, providing a viable option for electrochemical biosensing of Cu(II) and other metals in bioremediation^{22–25}.

¹DEI – Department of Electrical and Information Engineering, Polytechnic of Bari, Via E. Orabona 4, 70125 Bari, Italy. ²Department of Biosciences, Biotechnology and Environment, University of Bari, Via E. Orabona 4, 70125 Bari, Italy. ³Nottingham Ningbo China Beacons of Excellence Research and Innovation Institute, University of Nottingham Ningbo China, Ningbo, China. ⁴Department of Chemistry, University of Bari, Via E. Orabona 4, 70125 Bari, Italy. ⁵Institute for Physicochemical Processes (CNR-IPCF), National Research Council, Via E. Orabona 4, 70125 Bari, Italy. ⁶Ehtisham Wahid and Ohiemi Benjamin Ocheja have contributed equally to this work ✉email: enrico.marsili@nottingham.edu.cn

Currently, there is limited information on the bioelectrochemical response of yeast cells immobilized in PDA^{20,26}. In this work, *S. cerevisiae* cells were immobilized on disposable SPE. Microscopy and electrochemical characterization of the coatings were conducted using different carbon sources, non-inhibitory Cu(II) concentration, and several respiratory mutants in the presence of $K_3[Fe(CN)_6]$ as a redox mediator to enhance EET rate. PDA forms a homogeneous coating around yeast cells, enabling efficient EET. The high current output in the presence of the $K_3[Fe(CN)_6]$ show promises for the development of stable Cu(II) biosensors for monitoring bioremediation processes.

Materials and methods

SPE setup and materials

SPEs (Ref. TE100, Zensor, Taiwan) with 3 mm diameter carbon working electrode (WE), carbon counter electrode (CE), silver (Ag) pseudo-reference electrodes (RE), along with a multichannel potentiostat (Multipalmsens4, Palmsens, The Netherlands) were used for all bioelectrochemical experiments. Unless otherwise stated, all electrochemical potentials are reported against the Ag pseudo-reference electrode. Cell immobilization was achieved using dopamine hydrochloride (CAS: 62-31-7, Purity (HPLC): $\geq 97.5\%$) (Aladdin, China). Electrochemical measurements were carried out in an electrolyte solution containing a carbon source (glucose (Glu), glycerol (Gly), or ethanol (Eth)), $K_3[Fe(CN)_6]$, Magnesium dichloride ($MgCl_2$), and MOPS (3-(N-morpholino)propanesulfonic acid) buffer (Aladdin, China).

Yeast strains and growth conditions

The *S. cerevisiae* strains used in this study were *W303-1B (WT)* (MATa *ade2 leu2 his3 trp1 ura3*), the retrograde response derivative $\Delta rtg2$ ($\Delta rtg2::LEU2$) and the dysfunctional mitochondria derivative $\Delta hap4$ ($\Delta hap4::KanMX4$)²⁷. All strains were maintained and sub-cultured on yeast extract peptone dextrose (YPD) agar and grown in liquid YPD medium containing 1% yeast extract (w/w) (Aladdin, China), 2% bactopectone (w/w) (Gibco, Life Technologies, Waltham, MA, USA), and 2% glucose (w/w) (Sigma-Aldrich, St. Louis, MO, USA) at a shaking speed and temperature of 180 rpm and 30 °C. In some experiments, glucose was substituted with glycerol or ethanol at the same concentration. A Varioskan-LUX microplate reader (ThermoFisher Scientific, USA) was used to record yeast growth via absorbance measurement at 600 nm (OD_{600}). Before immobilization in PDA coatings, yeast cells were centrifuged twice at 4000 g (Sorvall ST 8R, ThermoFisher Scientific) and resuspended in 20 mM MOPS buffer, to remove extracellular debris and redox mediators that could affect the EET rate.

Assessment of *S. cerevisiae* tolerance to $K_3[Fe(CN)_6]$

The tolerance of *S. cerevisiae* to $K_3[Fe(CN)_6]$ was determined by incubating the cells with various concentrations of the compound in 2 mL test tubes. First, the stock culture of each strain, maintained at 4 °C, was aseptically transferred thrice to freshly prepared sterile YPD agar plate. Next, 5 mL of YPD medium was inoculated with a single colony from each strain and incubated overnight (16 h) at 30 °C and 180 rpm. The overnight cultures were then diluted with fresh YPD medium to a final OD_{600} of 0.05. $K_3[Fe(CN)_6]$ stock solution was added to each tube containing YPD medium to obtain a final concentration ranging from 25 to 100 μM . Then, 800 μL of the culture was transferred into each well of a 48-well microtiter plate. Wells containing culture without $K_3[Fe(CN)_6]$ and YPD medium only were used as controls and blanks, respectively. The cells were incubated in the microplate reader at 30 °C and 180 rpm for 48 h, with cell growth monitored by measuring OD_{600} every hour throughout the incubation.

Effects of Cu(II) on growth and viability of *S. cerevisiae*

The effect of Cu(II) on yeast cell growth and viability was assessed as follows: 5 mL YPD medium was inoculated with an axenic colony of each strain and incubated overnight (16 h) in 50 mL flasks at 30 °C and 180 rpm in a shaking incubator. The overnight cultures were diluted with fresh YPD medium to a final OD_{600} of 0.05 in flasks containing 50 mL sterile YPD medium supplemented with varying concentrations of $CuSO_4$ (10–100 μM). Culture without $CuSO_4$ and medium without cells were used as controls and blanks, respectively. The cultures were incubated 30 °C and 180 rpm for 48 h, and cell growth was monitored by measuring OD_{600} every hour throughout the incubation.

Cell viability was assessed by colony forming unit (CFU) counting on YPD agar plates. During incubation, 100 μL of aliquot was taken from each culture every 2 h until the end of the exponential growth phase (18 h). This was serially diluted in sterile milliQ water, inoculated onto YPD agar plates and incubated at 30 °C for 48 h. Colonies formed on each plate after incubation were counted, with the number of untreated colonies considered 100%, and the viability of treated colonies calculated as a percentage of untreated cells²⁸.

Coatings preparation

For electrochemical analysis, *S. cerevisiae* cells and dopamine hydrochloride were used to prepare coatings following previously published protocols²⁶. Briefly, cells were pre-inoculated overnight in YPD medium and then incubated in fresh YPD. The culture was centrifuged and resuspended in 20 mM MOPS buffer at pH 7 to enable self-polymerization of PDA with 50 mM glucose as a carbon source. This suspension was mixed with 10 mM dopamine hydrochloride solution in 1:1 ratio and magnetically stirred under aerobic conditions for 1 h to obtain a homogeneous solution. Following aerobic polymerization, 5 μL of the solution was drop-cast on the 3 mm WE surface of the SPE and left to dry at a controlled temperature of 26 ± 1 °C for 30 min. Electrochemical polymerization was performed with 20 repeated cyclic voltammetry (CV) scans between -0.3 and $+0.5$ V with a scan rate of 20 $mV s^{-1}$. The number of cycles was optimised to avoid formation of oversized PDA coating (data not shown). PDA coatings were characterized using scanning electron microscopy (SEM), CV, chronoamperometry

(CA), and EIS. Control experiments were performed using the same coatings preparation procedures with dead cells (cells were heat-killed by placing them in a hot water bath for 1 h at 100 °C) and PDA-only coatings. All experiments were performed at fixed temperature of 26 ± 1 °C in 20 mL scintillation vials containing 18 mL electrolyte solution (20 mM MOPS buffer, pH 5 to avoid precipitation of copper hydroxide), 10 mM MgCl_2 , 50 mM glucose, and 50 μM $\text{K}_3[\text{Fe}(\text{CN})_6]$ under aerobic conditions. CuSO_4 (0 to 100 μM) was added to selected experiments and the vials were magnetically stirred at 100 rpm for 120 s to ensure a homogeneous solution.

Field emission scanning electron microscope (FE-SEM)

The morphology of PDA coating was evaluated using a field emission scanning electron microscope (FE-SEM) (Sigma VP, ZEISS, Germany). Coatings were prepared as described above and cut to fit the size of stub/sample holder. Samples were fixed on the stub using conductive double-sided tape and gold-coated using an ion sputtering apparatus (SBC-12, KYKY, China) for 20–40 s at 5–10 mA. The samples were observed at a magnification of 1000 X with an area width of 3 to 10 mm under a vacuum pressure of 10 Pa. Other inspecting conditions such as signal collected (in-lens), conductor status (standard) and acceleration voltage (3 or 5 kV) were adjusted to obtain high-quality images.

Data analysis

All experiments were performed at least in triplicates. Separate cell cultures were prepared under the same conditions to obtain independent biological replicates. All electrochemical experiments were also performed using new SPE and sterilized electrochemical cells. For each dataset, the mean and standard deviation of experiments with three independent biological replicates ($n = 3$) are reported.

Results and discussion

Field emission scanning electron microscope (FE-SEM)

Figure 1a, b displays the bare and PDA-coated WE surface, respectively. The arrow in Fig. 1a indicates rough surface patches on the surface of SPE. The bare WE surface roughness favours coating adhesion and cell immobilization, which result in stable current output with time and better biosensor performance²⁹. In Fig. 1b the arrow shows microstructures leading to formation of a smooth and uniform layer over the WE.

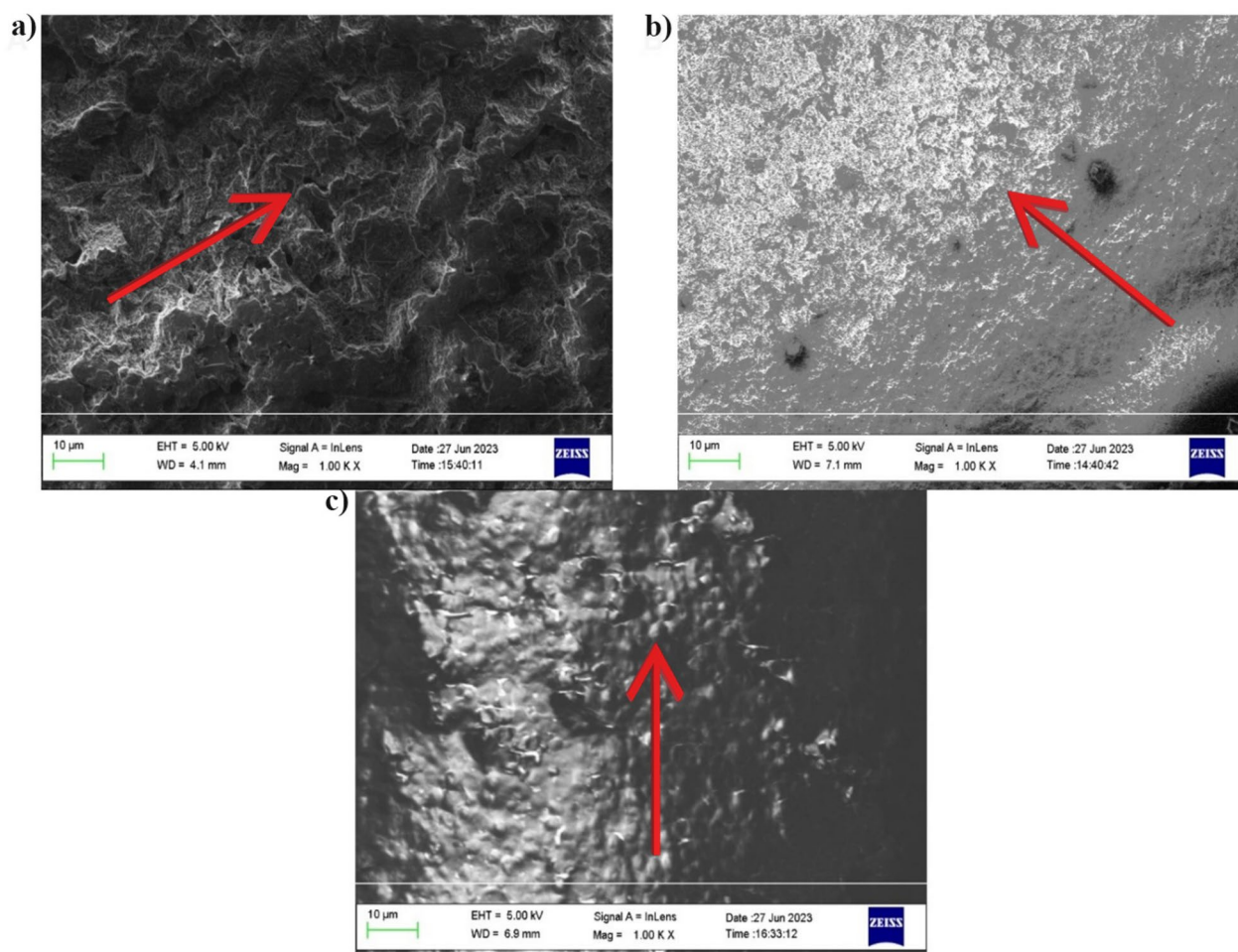


Fig. 1. (a) Bare surface of WE, (b) PDA-coated WE, (c) *S. cerevisiae* cells immobilized in PDA on the WE.

The microstructures observed in the PDA coating may result from the self-polymerization of PDA and could contribute to enhancing cell adhesion and homogeneous distribution in the coating preparation.

Figure 1c shows *S. cerevisiae* cells embedded within the PDA coating on the WE surface. The arrow displays cells that appear as round beads within the PDA matrix, indicating effective immobilization and homogeneous cell distribution, without the formation of cell clusters. The image is representative of the whole coated surface, as the uniform PDA coverage and consistent cell distribution are observed across all the WE tested.

Effects of $K_3[Fe(CN)_6]$ on the growth of *S. cerevisiae*

The effect of the redox mediator $K_3[Fe(CN)_6]$ on the growth of *S. cerevisiae* WT and mutant cells was determined using a multi-well plate assay. The results indicated that the growth rates were not significantly affected by the redox mediator at the concentrations tested (Figure S1). $K_3[Fe(CN)_6]$ has been used both in microbial fuel cells (MFC) and electrochemical biosensors to increase EET rate from biofilms to electrodes^{30,31}. For example, a *S. cerevisiae* MFC showed improved performance when 50 mM $K_3[Fe(CN)_6]$ was added as external mediator³⁰. Despite its mild toxicity, $K_3[Fe(CN)_6]$ was successfully employed as redox mediator with fungi *Candida albicans*³² at 100 μ M concentration. With respect to another biocompatible redox mediator like 2-hydroxy-1,4-naphthoquinone (HNQ), $K_3[Fe(CN)_6]$ is more stable and has a faster turnover rate^{33,34}. Therefore, 50 μ M $K_3[Fe(CN)_6]$ was used in all electrochemical experiments carried out in this study.

Influence of Cu(II) on the growth and viability of *S. cerevisiae*

The ability to replicate and develop into colonies remains the gold standard for estimating microbial cell viability³⁵. Thus, growth analysis and CFU counting of *S. cerevisiae* strains exposed to various Cu(II) concentrations were carried out according to standard CFU protocols. The results showed no significant difference in the growth rate of the three strains tested in the presence and absence of Cu(II) (Fig. 2 and Figure S2). Viability decreased with increasing concentrations of $CuSO_4$ in each strain. However, the differences are not statistically significant (Tukey's test, $p < 0.05$). Considering that ISO 10993-5:2009 standard define 30% viability decrease as the threshold for cytotoxicity^{36,37}, we conclude that 100 μ M $CuSO_4$ is a suitable upper limit concentration for the proposed biosensor.

Depending on the concentration, Cu(II) can either play a key role in enzymatic metabolic processes or exert cytotoxic effects, causing cellular damage and loss of viability, especially during bioproduction processes such as fermentation^{24,38}. In *S. cerevisiae*, increased level of the metalloenzyme superoxide dismutase (SOD) is directly linked to the presence of Cu(II) in the environment. Copper, as an inorganic cofactor, aids SOD in controlling reactive oxygen species levels, thereby protecting the cells from oxidative stress³⁹. This is supported by increased SOD1 mRNA transcript levels in the presence of bathocuproine sulphonate, a Cu(II) chelator⁴⁰. However, the level of viability maintained in the presence of Cu(II) varies widely among *S. cerevisiae* strains, depending on factors such as habitat of isolation and genotype. For example, YPD medium supplemented with 1 mM Cu(II) did not significantly affect the growth rate or viability of six different yeast strains comprising four *S. cerevisiae* and two *Pichia pastoris*⁴¹, whereas *S. cerevisiae* BH8 exposed to 0.5 mM $CuSO_4$ showed enhanced growth in another study³⁸. Consistent with our result, OD_{600} measurements showed no effect on the growth of *S. cerevisiae* strains S288c, AWRI1631, RM11, and YJM339 when exposed to 50 and 100 μ M $CuSO_4$ ²⁸. Fungi employ two primary metal detoxification mechanisms: surface binding (biosorption) or intracellular uptake during metabolism (bioaccumulation)⁴², and these traits vary widely among *S. cerevisiae* strains²⁴. The low impact of Cu(II) on yeast viability in the 0–100 μ M concentration range suggests its potential for electrochemical detection. Previous studies have developed biosensors using immobilized yeast cells for Cu(II). Genetically modified *S. cerevisiae* cells immobilized in alginate beads have been used to detect Cu(II) in the 1–100 μ M range in drinking water and wastewater⁴³. Our findings are consistent with previous studies, suggesting Cu(II) detection can be achieved electrochemically using viable *S. cerevisiae* cells immobilized in PDA coatings.

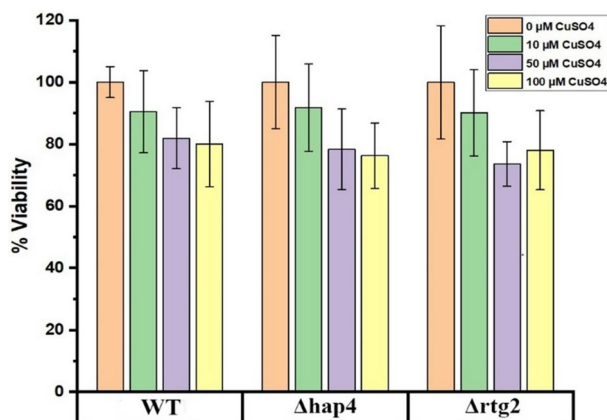


Fig. 2. Viability of WT, $\Delta hap4$ and $\Delta rtg2$ *S. cerevisiae* strains incubated for 18 h in YPD medium supplemented with 10–100 μ M $CuSO_4$.

Electrochemical analysis

The effect of CuSO_4 (0–100 μM) on the electroactivity of exponentially growing *S. cerevisiae* WT, $\Delta hap4$ and $\Delta rrg2$ cells was analyzed through PDA coatings using CV, CA and EIS.

Cyclic voltammetry

CV is a diagnostic technique for assessing the metabolic activity of attached cells^{44–46}. Dead cells, PDA-only, and viable cells immobilized on the WE surface were characterized at 2 mV s^{-1} scan rate between -0.30 and 0.52 V (Figure S3). After 14 h of growth, control experiments with PDA-only coating and dead yeast cells in PDA showed lower current density (j) than viable yeast cells in PDA. However, no distinct redox peaks were observed.

Electrochemical impedance spectroscopy

EIS was used to study response of four samples: viable *S. cerevisiae* WT cells immobilized in PDA with redox mediator (Sample 1), without redox mediator (Sample 2); PDA-only without redox mediator (Sample 3), and dead *S. cerevisiae* WT cells immobilized in PDA without redox mediator (Sample 4). Potentiostatic EIS was performed between -100 and 400 mV with a step potential of 50 mV in the 50 kHz – 0.05 Hz frequency range. EIS data were fitted with a two time-constant equivalent circuit using EC-Lab V11.61 (Bio-Logic, France). The Nyquist plot (Fig. 3a and Figure S7)) showed increasing real and imaginary components from Sample 1 to sample 4, indicating reduced impedance during EET in the presence of viable cells and redox mediator. For all samples impedance increase with the applied potential from -100 mV to 400 mV . Depressed, incomplete semi-circles for each sample indicated non-ideal capacitance⁴⁷. Figure 3b and Figure S8 shows the Bode phase plot, with two distinct features at $f \sim 100 \text{ Hz}$ and $f \sim 1 \text{ Hz}$. The feature at $f \sim 1 \text{ Hz}$ represent charge transfer and

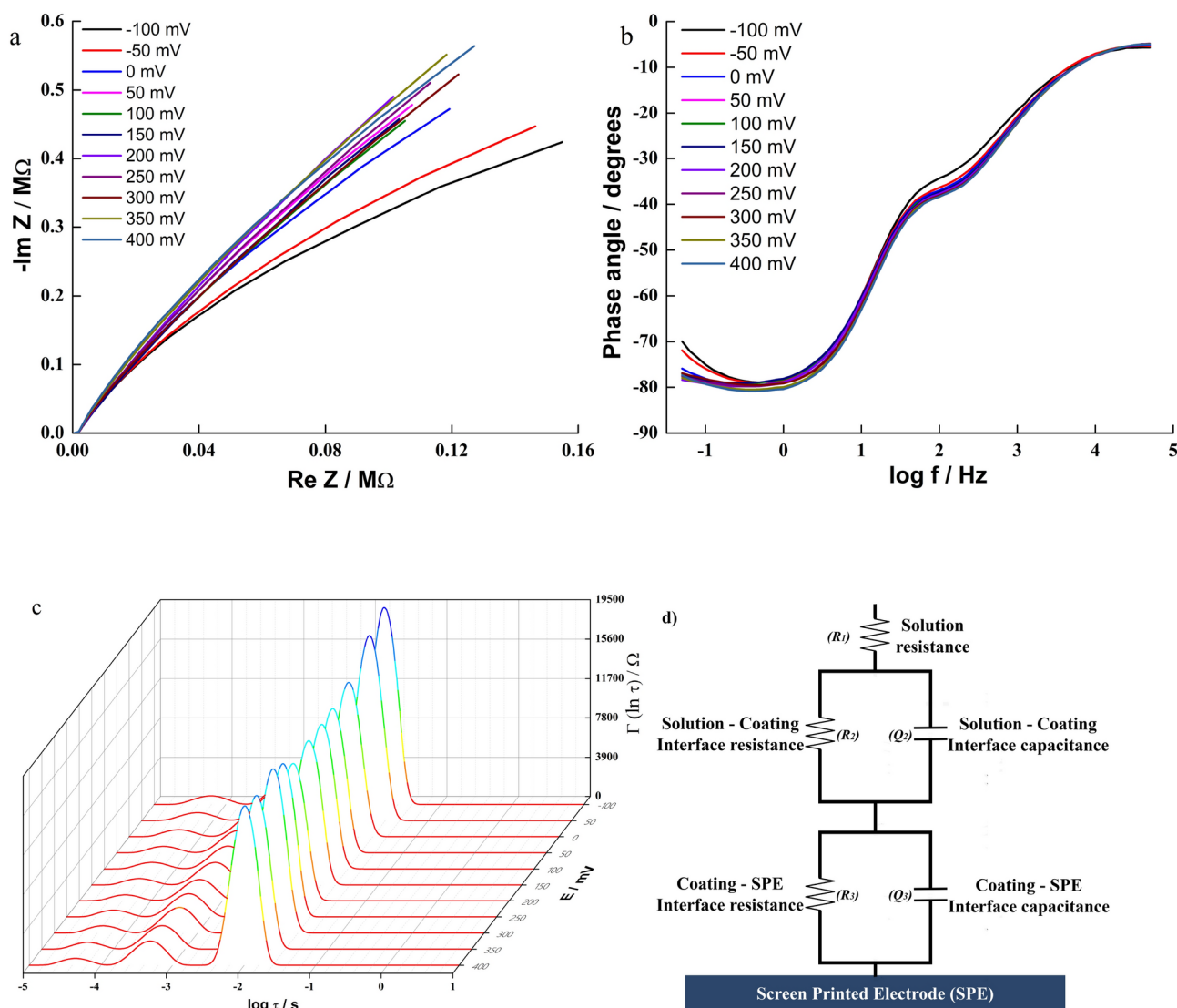


Fig. 3. (a) Nyquist plot; (b) Bode phase plot; (c) DRT plot of Sample 1 between -100 and 400 mV with a step potential of 50 mV ; (d) Schematic of the equivalent circuit.

double-layer capacitance on the coating-electrode interface, while the feature at $f \sim 100$ Hz describes charge accumulation on coating-electrolyte interface⁴⁸.

The phase angle never reached 90° , indicating non-ideal capacitive behavior, which can be modeled as a constant phase element (CPE)⁴⁷, explaining the depressed semicircles observed in the Nyquist plot. The experimental EIS data was analyzed using the distribution function of relaxation times (DRT) and the corresponding time constants were calculated with an open-source Matlab-based DRT tool prior to modeling with equivalent circuit fitting (Fig. 3c and Figure S9)⁴⁹. From DRT analysis, a leftward shift and reduction in time constants with increasing voltages for all samples was observed. This typically represents faster relaxation times, meaning that the electrochemical reactions or charge transfer processes involving the immobilized yeast cells are occurring more rapidly, indicating that the PDA layer provides a stable and conductive interface for the yeast cells⁵⁰.

Given that the DRT analysis and phase angle revealed two distinct time constants, a Randles equivalent circuit comprising the resistance of electrolyte in series with two resistor-CPE circuits (Fig. 3d) was selected to represent the system⁵¹. In the equivalent circuit, R_1 represent the electrolyte resistance R_e , Q_2 and α_2 represent the CPE at the solution-coating interface, and R_2 represents the charge transfer resistance R_{ct} at the same interface. Q_3 , α_3 and R_3 similarly model the non-ideal capacitance and charge transfer resistance at the coating-electrode interface⁵¹. The use of CPE accounts for the irregularities on the surface due to the roughness of the SPE and inhomogeneities in the coating⁵². Since CPE was employed in the model, the effective capacitance was calculated using the Brug Eq. (1). Brug's equation account for both the electrolyte resistance and the behavior associated with surface distributions^{48,53,54}.

$$C_{eff} = Q^{1/\alpha_3} \left(\frac{R_e R_{ct}}{R_e + R_{ct}} \right)^{(1-\alpha_3)/\alpha_3} \quad (1)$$

where R_e is the electrolyte resistance and R_{ct} , Q_3 , and α_3 represent the CPE parameters for the coating-electrode interface.

The analysis of R_e calculated from the equivalent circuit fitting showed variation across samples and with the applied potential (Figure S6), indicating that electrolyte diffusion in the coating depends on its composition and activity. Moreover, no significant reduction was observed in R_1 in the presence of mediator (Figure S6). Figure 4 shows the R_{ct} for the coating-electrode interface calculated from the equivalent circuit fitting for all samples at different potentials. The interfacial resistance for sample 4 (dead cells) was higher than samples 2 and 1 (viable cells), while sample 3 had the lowest resistance. This effect suggests a facilitated charge-limited process and confirms the increased EET from the cells in sample 2 and 1. In contrast to interfacial resistance, effective capacitance showed an inverse trend, with sample 1 and 2 (viable cells) displaying higher capacitance in the fitted data compared to sample 4 (dead cells). This indicates the formation of a space charge layer in sample 1 and 2 (viable cells) due to higher EET, resulting in double-layer capacitance at electrode-biofilm interface. These results are consistent with our hypothesis and with the results obtained from CV and CA as well.

Chronoamperometry

In long-term experiments (e.g., 24–48 h), the current output is due to the growth and respiration of the electricigens⁵⁵. For short-term experiments with coatings, where cell growth can be neglected, the current output can be interpreted as steady-state electrode respiration of the immobilized cells. Thus, short-term CA is a suitable method to determine the effects of environmental conditions, nutrient concentrations, genetic modifications, pollutants, etc. on the cell respiration rate. In an initial set of experiments, *S. cerevisiae* WT cells were grown in

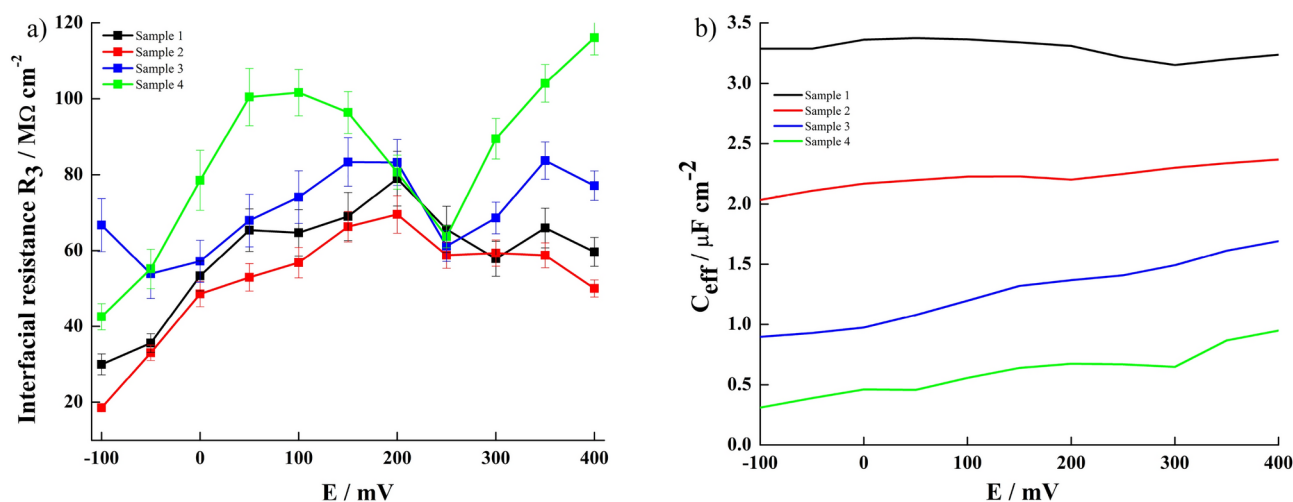


Fig. 4. (a) Interfacial resistance for all samples. (b) Effective capacitance for all samples.

rich medium with glucose as fermentative carbon source and glycerol and ethanol as non-fermentative carbon sources. Unlike glucose, which is preferentially metabolized by yeast cells even in the presence of oxygen (glucose catabolite repression), glycerol and ethanol stimulate respiration. Results showed that the current output was significantly higher under respiratory metabolism compared to fermentative metabolism (Fig. 5).

Interestingly, it was reported that *S. cerevisiae* respired aerobically in the mitochondria in the presence of glycerol as a carbon source, producing 30% more ATP than in a medium containing glucose as the carbon source⁵⁶. Vasylykova et al. (2015) also demonstrated that the medium supplemented with glycerol or ethanol as carbon sources lead to 6.9- and 3.3-fold increase in metabolic rates, respectively, compared to media containing glucose⁵⁷. Although no significant difference was recorded in the SOD activity of the strains utilizing each of these carbon sources, catalase activity was found to be 3.3% higher in the glycerol medium relative to the glucose medium. Relative growth data under these conditions suggest that copper has a stimulatory effect in glycerol or ethanol medium (Figure S4 and S5) according to⁵⁸. Beyond its positive effect on respiratory rate, copper can also ameliorate oxidative stress. As previously reported, trace amount of Cu(II) can increase SOD activity. This, combined with the high catalase activity in the presence of glycerol, could result in a more balanced redox state, leading to the increase in current output⁵⁹.

The CA results were compared at 2500 s, where the current output reached a steady state for all samples, and the EET rate increase by about 30% for cells cultured in glycerol or ethanol at almost all concentrations of CuSO_4 , compared to glucose. However, at all concentrations of CuSO_4 , the current output decreased in all samples (Fig. 6 and Table S1), indicating that short-term exposure to CuSO_4 causes a rapid change in extracellular respiration rate. Thus, PDA coatings can be used to prepare biosensors for the rapid detection of respiratory stress agents, such as toxic metals and other pollutants. The data obtained from the dose-dependent response of the coating (Fig. 6) was analysed for linear fitting, and the LOD was calculated according to the $3S_b/m$ criterion, where m is the slope of the linear range and S_b the standard deviation of the intercept⁶⁰. Interestingly, while glucose showed an LOD of 2.2 μM , the higher respiration rate with glycerol and ethanol as carbon sources resulted in lower LODs (1.8 and 1.4 μM , respectively), with high sensitivity for CuSO_4 (Table S3).

Having observed that respiratory metabolism might affect electrical cell response, CA was performed on two mutant strains, $\Delta hap4$ and $\Delta rtg2$, lacking the catalytic subunit of the *hap2-5* transcriptional complex required for the control of the tricarboxylic acid (TCA) cycle and electron transport, and the upstream regulator of the mitochondrial retrograde pathway, respectively. The three strains were cultured in medium containing glucose as the sole carbon source. Both mutations improved the EET response by more than 80% without CuSO_4 . However, in the presence of CuSO_4 , the current output increase was approximately 30% for $\Delta hap4$ and become negligible for the $\Delta rtg2$ strain (Figs. 7, 8 and Table S2), indicating a perturbation in the cell's metabolic state that could be associated with Cu (II) induced stress. These observations align with cell growth data, which show that copper can enhance cell growth in both mutants compared to WT (Figure S4). Conversely, the increased EET response in the presence of copper could be due to reduced oxidative stress in the mutants. Control experiments with PDA coatings containing heat-killed cells and PDA-only coatings showed negligible current output.

The higher rate of respiration observed in $\Delta hap4$ and $\Delta rtg2$ agrees with previous reports⁶¹ and could be due to the higher mitochondrial mass, especially in $\Delta hap4$, where growth appeared accelerated compared to WT cells in the absence of stress. Additionally, the higher copper resistance in both mutant strains may be an effect of dysfunctional mitochondria⁴³.

Overall, this confirms an interplay between *rtg2* and *hap4* in controlling mitochondrial function⁶². The higher respiration rate in $\Delta hap4$ and $\Delta rtg2$ strains grown on glucose as the carbon source translate into a lower LOD and higher sensitivity for CuSO_4 (Table S4). Moreover, the results obtained in this work with biosensors prepared using metabolic and genetic manipulations immobilized on SPE showed improvement in all aspects

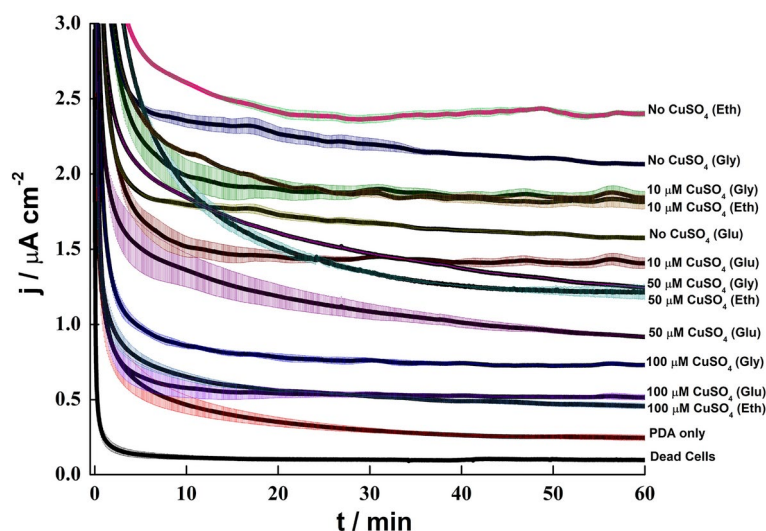


Fig. 5. CA of PDA coating with *S. cerevisiae* WT cells with glucose, glycerol, and ethanol as the carbon source at 0.4 V, with different concentration of CuSO_4 (0, 10, 50, 100 μM) under aerobic conditions.

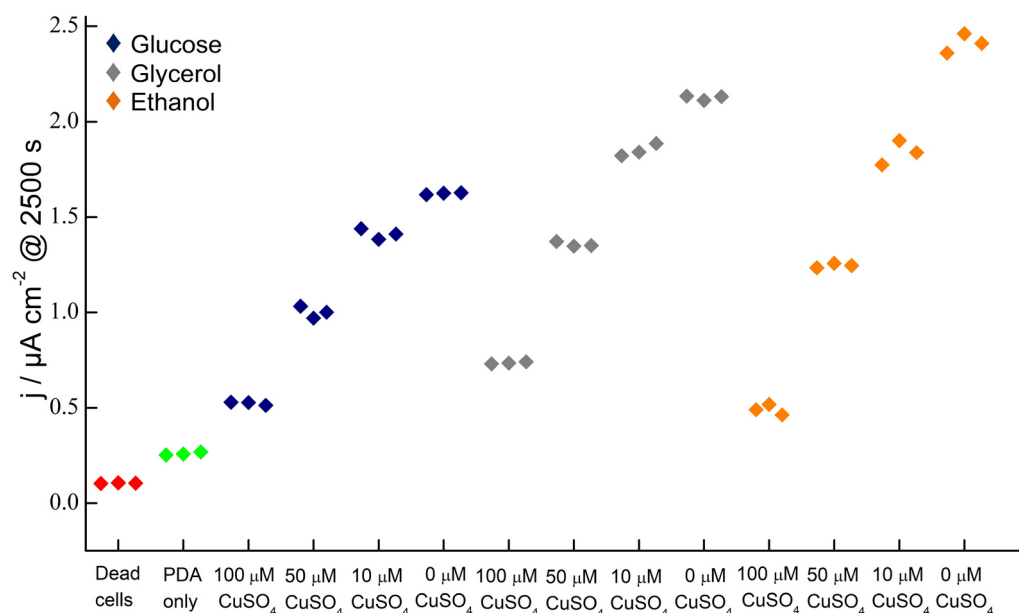


Fig. 6. Current density of PDA coating with *S. cerevisiae* WT cells with glucose, glycerol, and ethanol as the carbon source with different concentration of CuSO_4 (0, 10, 50, 100 μM) under aerobic conditions after 2500 s of incubation at $E = 0.4$ V.

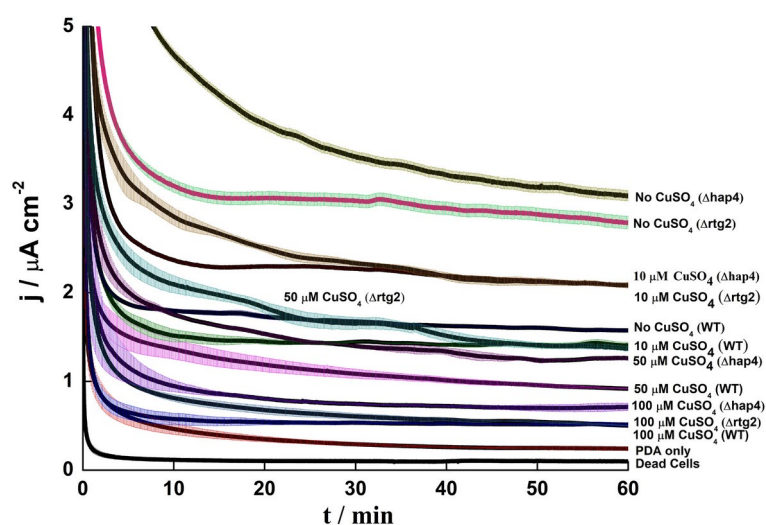


Fig. 7. CA of Current density of PDA coating with *S. cerevisiae* WT, Δhap4 and Δrtg2 cells at 0.4 V with different concentration of CuSO_4 (0, 10, 50, 100 μM) under aerobic conditions.

such LoD, R^2 and sensitivity in comparison to the results obtained by glassy carbon bioelectrode²⁶. The current set of biosensors provided at least 10 percent higher in LoD, improved R^2 (except ethanol in case of different carbon sources and Δhap4 in case of mutant) as well as a minimum of twofold increase in sensitivity²⁶. Looking at the CA traces, either two or three phases can be observed (Figs. 5 and 7): (a) a rapid capacitive discharge in the initial 5 min; (b) a slow decrease of the current output, which lasts longer at low CuSO_4 concentrations; and (c) a plateau phase, during which the current remain stable over time. Virtually no current was observed for dead cells, indicating the biological origin of the current output. The current output for dead cells was even lower than that of PDA only, likely due to the polyelectrolyte nature of PDA, which facilitate EET⁶³.

The CuSO_4 concentration of 100 μM is likely close to the minimum inhibitory concentration (MIC)^{64–66}, meaning cells are slowly dying or being inhibited under these conditions. For practical applications, the concentration of the analyte should be kept lower than the MIC to avoid damaging the sensing element. The comparison between CFU counting and CA analysis indicates that both methods show similar trends. However, in the case of CFU counting, growth inhibition is minimal, with a slight decrease in percentage viability only

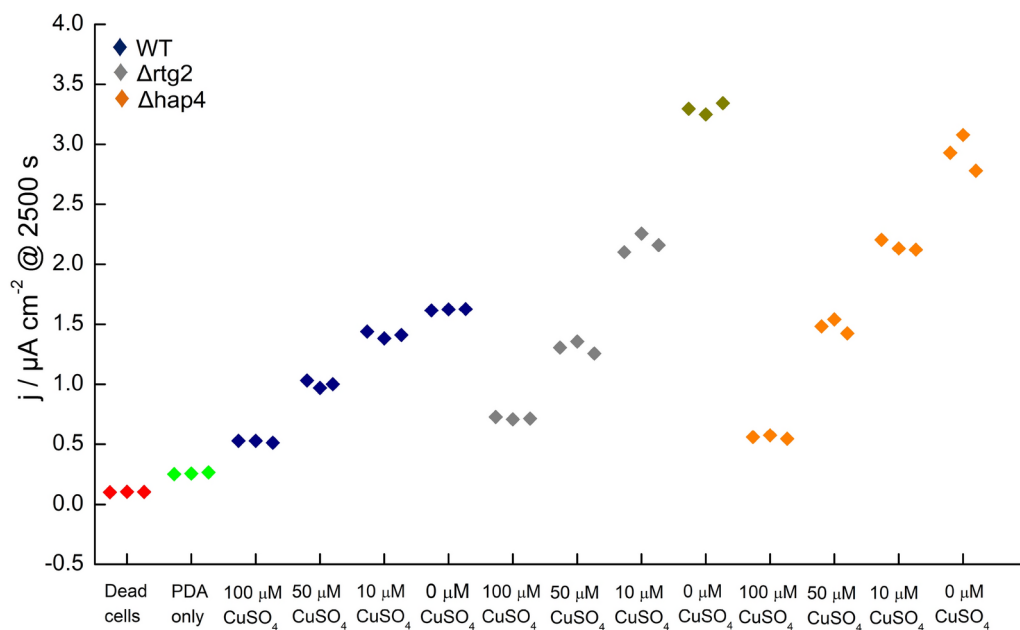


Fig. 8. Current density of PDA coating with *S. cerevisiae* WT, $\Delta hap4$ and $\Delta rtg2$ cells at 0.4 V with different concentration of $CuSO_4$ (0, 10, 50, 100 μM) under aerobic conditions after 2500 s of incubation.

observed after 18 h of exposure (Fig. 2). Thus, PDA coatings offer better sensitivity and more rapid detection compared to conventional growth-based assays.

Conclusions

This study focuses on creating a sustainable and economical biosensor by coating viable *S. cerevisiae* cells in polydopamine on a screen-printed electrode, to detect Cu(II), with potential applications in bioremediation. The immobilization process preserves the yeast cells' metabolic functionality and stability, enabling effective electrochemical analysis over time through chronoamperometry. The use of disposable carbon screen-printed electrodes improves the sensor's portability and its detection accuracy with respect to conventional carbon rod electrode for laboratory studies. Scanning electron microscopy and electrochemical impedance spectroscopy were applied to validate these enhancements, providing further information on the electron transfer process in the biocoating. Further study will employ genetically modified yeast cells to detect specific metal contaminants for environmental monitoring and bioremediation applications.

Data availability

The full dataset for this work can be requested via email to Enrico Marsili (enrico.marsili@nottingham.edu.cn).

Received: 8 October 2024; Accepted: 13 January 2025

Published online: 21 January 2025

References

- Clark, L. C. & Lyons, C. Electrode systems for continuous monitoring in cardiovascular surgery. *Ann N. Y. Acad. Sci.* **102**, 29–45 (1962).
- Labib, M., Sargent, E. H. & Kelley, S. O. Electrochemical methods for the analysis of clinically relevant biomolecules. *Chem Rev* **116**(16), 9001–9090 (2016).
- Wu, J. et al. Biomedical and clinical applications of immunoassays and immunosensors for tumor markers. *TrAC Trends Anal. Chem.* **26**, 679–688 (2007).
- Minteer, S. D. Advances in electroanalytical chemistry. *J Am Chem Soc* **140**(8), 2701–2703 (2018).
- Adeniran, A., Sherer, M. & Tyo, K. E. Yeast-based biosensors: design and applications. *FEMS Yeast Res* **15**(1), 1–15 (2015).
- Jarque, S. et al. Yeast biosensors for detection of environmental pollutants: Current state and limitations. *Trends Biotechnol* **34**(5), 408–419 (2016).
- Martin-Yken, H. Yeast-based biosensors: current applications and new developments. *Biosensors (Basel)* **10**(5) (2020).
- Roda, A. et al. Analytical strategies for improving the robustness and reproducibility of bioluminescent microbial bioreporters. *Anal Bioanal Chem* **401**(1), 201–211 (2011).
- Lian, J., Mishra, S. & Zhao, H. Recent advances in metabolic engineering of *Saccharomyces cerevisiae*: New tools and their applications. *Metab Eng* **50**, 85–108 (2018).
- Turcotte, B. et al. Transcriptional regulation of nonfermentable carbon utilization in budding yeast. *FEMS Yeast Res* **10**(1), 2–13 (2010).
- Raghavulu, S. et al. *Saccharomyces cerevisiae* as anodic biocatalyst for power generation in biofuel cell: Influence of redox condition and substrate load. *Bioresour Technol* **102**, 2751–2757 (2010).
- Sayed, E. et al. Yeast extract as an effective and safe mediator for the Baker's-Yeast-based microbial fuel cell. *Ind. Eng. Chem. Res.* **54**, 3116–3122 (2015).

13. Lovley, D. Electromicrobiology. *Annu. Rev. Microbiol.* **66**, 391–409 (2012).
14. Xie, X., Criddle, C., and Cui, Y. Design and fabrication of bioelectrodes for microbial bioelectrochemical systems. *Energy Environ. Sci.* **8** (2015).
15. Holten-Andersen, N. & Waite, J. H. Mussel-designed protective coatings for compliant substrates. *J Dent Res* **87**(8), 701–709 (2008).
16. Papov, V. et al. Hydroxyarginine-containing polyphenolic proteins in the adhesive plaques of the marine mussel *mytilus edulis*. *J. Biol. Chem.* **270**, 20183–20192 (1995).
17. Liu, Y., Ai, K., and Lu, L. Polydopamine and its derivative materials: Synthesis and promising applications in energy, environmental, and biomedical fields. *Chem. Rev.* **114** (2014).
18. Yang, S. H. et al. Mussel-inspired encapsulation and functionalization of individual yeast cells. *J Am Chem Soc* **133**(9), 2795–2797 (2011).
19. Fakhruddin, R. et al. Cyborg cells: Functionalisation of living cells with polymers and nanomaterials. *Chem. Soc. Rev.* **41**, 4189–4206 (2012).
20. Wang, L. et al. Polydopamine nanocoated whole-cell asymmetric biocatalysts. *Chem Commun (Camb)* **53**(49), 6617–6620 (2017).
21. Du, Q., et al. Protection of electroactive biofilm from extreme acid shock by polydopamine encapsulation. *Environ. Sci. Technol. Lett.* **4** (2017).
22. Nogueiro, R. C. et al. Sequential extraction and availability of copper in Cu fungicide-amended vineyard soils from Southern Brazil. *J Hazard Mater* **181**(1–3), 931–937 (2010).
23. Claus, H. Copper-containing oxidases: occurrence in soil microorganisms, properties, and applications, pp. 281–313 (2010).
24. Capece, A. et al. Yeast starter as a biotechnological tool for reducing copper content in wine. *Front Microbiol* **8**, 2632 (2017).
25. García Esparza, M. et al. Copper content of grape and wine from Italian farms. *Food Addit. Contaminants* **23**, 274–280 (2006).
26. Benjamin Ocheja, O. et al. Polydopamine-immobilized yeast cells for portable electrochemical biosensors applied in environmental copper sensing. *Bioelectrochemistry* **157**, 108658 (2024).
27. Guaragnella, N. et al. Yeast growth in raffinose results in resistance to acetic-acid induced programmed cell death mostly due to the activation of the mitochondrial retrograde pathway. *Biochim Biophys Acta* **1833**(12), 2765–2774 (2013).
28. Rong-Mullins, X. et al. Proteomic and genetic analysis of the response of *S. cerevisiae* to soluble copper leads to improvement of the antimicrobial function of cellulosic copper nanoparticles. *Metallomics* **9**(9), 1304–1315 (2017).
29. Police Patil, A. V., et al. Recent advances in electrochemical immunosensors with nanomaterial assistance for signal amplification. *Biosensors (Basel)*. **13**(1) (2023).
30. Gunawardena, A., Fernando, S. & To, F. Performance of a yeast-mediated biological fuel cell. *Int J Mol Sci* **9**(10), 1893–1907 (2008).
31. Tharali, A., Sain, N. & Osborne, J. Microbial fuel cells in bioelectricity production. *Front. Life Sci.* **9**, 1–15 (2016).
32. Olaifa, K. et al. Electroanalysis of *Candida albicans* biofilms: A suitable real-time tool for antifungal testing. *Electrochimica Acta* **389**, 138757 (2021).
33. Wark, A. W. et al. Bioaffinity detection of pathogens on surfaces. *J Ind Eng Chem* **16**(2), 169–177 (2010).
34. Santoro, C., et al. Sub-toxic concentrations of volatile organic compounds inhibit extracellular respiration of *Escherichia coli* cells grown in anodic bioelectrochemical systems. *Bioelectrochemistry*. **112** (2016).
35. Meyer, C. T. et al. A high-throughput and low-waste viability assay for microbes. *Nat Microbiol* **8**(12), 2304–2314 (2023).
36. Costa, E. et al. Spent yeast waste streams as a sustainable source of bioactive peptides for skin applications. *Int. J. Mol. Sci.* **24**, 2253 (2023).
37. Vicensoto Moreira, M., et al. Ascorbic acid as a modulator of inflammatory response against *Candida albicans*. *Future Microbiol.* **19** (2024).
38. Sun, X. et al. Effect of high Cu²⁺ stress on fermentation performance and copper biosorption of *Saccharomyces cerevisiae* during wine fermentation. *Food Sci. Technol.* **39** (2018).
39. Berterame, N. M. et al. Copper homeostasis as a target to improve *Saccharomyces cerevisiae* tolerance to oxidative stress. *Metab Eng* **46**, 43–50 (2018).
40. Montllor-Albalade, C. et al. Extra-mitochondrial Cu/Zn superoxide dismutase (Sod1) is dispensable for protection against oxidative stress but mediates peroxide signaling in *Saccharomyces cerevisiae*. *Redox Biol* **21**, 101064 (2019).
41. Vulpe, C. et al. Copper accumulation efficiency in different recombinant microorganism strains available for bioremediation of heavy metal-polluted waters. *Int. J. Mol. Sci.* **24**, 7575 (2023).
42. Tufail, M. et al. Recent advances in bioremediation of heavy metals and persistent organic pollutants: A review. *Sci. Total Environ.* **850**, 157961 (2022).
43. Vopálenková, I., Váchová, L., and Palkova, Z. New biosensor for detection of copper ions in water based on immobilized genetically modified yeast cells. *Biosens. Bioelectron.* **72** (2015).
44. Marsili, E. et al. Microbial biofilm voltammetry: direct electrochemical characterization of catalytic electrode-attached biofilms. *Appl Environ Microbiol* **74**(23), 7329–7337 (2008).
45. Babauta, J. et al. Electrochemically active biofilms: Facts and fiction. A review. *Biofouling* **28**(8), 789–812 (2012).
46. Chalenko, Y. et al. Electrochemistry of *Escherichia coli* JM109: Direct electron transfer and antibiotic resistance. *Biosens. Bioelectron.* **32**, 219–223 (2011).
47. Pires, L. et al. Online monitoring of biofilm growth and activity using a combined multi-channel impedimetric and amperometric sensor. *Biosens Bioelectron* **47**, 157–163 (2013).
48. Hirschhorn, B. et al. Determination of effective capacitance and film thickness from constant-phase-element parameters. *Electrochimica Acta* **55**, 6218–6227 (2010).
49. Wan, T., et al. Influence of the discretization methods on the distribution of relaxation times deconvolution: Implementing radial basis functions with DRTtools. *Electrochimica Acta* **184** (2015).
50. Astorga, S. E., Hu, L. X., Marsili, E. & Huang, Y. Ordered micropillar array gold electrode increases electrochemical signature of early biofilm attachment. *Mater. Des.* **185**, 108256 (2020).
51. Astorga, S. et al. Electrochemical signature of *Escherichia coli* on Ni micropillar array electrode for early biofilm characterization. *ChemElectroChem* **6**, 4674–4680 (2019).
52. Salazar, P., Martín, M., and González-Mora, J. In situ electrodeposition of cholesterol oxidase-modified polydopamine thin film on nanostructured screen printed electrodes for free cholesterol determination. *J. Electroanal. Chem.* **837** (2019).
53. Domínguez-Benetton, X. et al. The accurate use of impedance analysis for the study of microbial electrochemical systems. *Chem. Soc. Rev.* **41**, 7228–7246 (2012).
54. Samantha Michelle, G. et al. On the use of a constant phase element (CPE) in electrochemistry. *Curr. Opin. Electrochem.* **36**, 101133 (2022).
55. Sánchez, C. et al. Microbial electrochemical technologies: Electronic circuitry and characterization tools. *Biosens Bioelectron* **150**, 111884 (2020).
56. Maslanka, R., Zdrag-Tecza, R., and Kwolek-Mirek, M. Linkage between carbon metabolism, redox status and cellular physiology in the yeast. *Genes (Basel)* **11**(7) (2020).
57. Vasylykova, R., Petriv, N. & Semchysyn, H. Carbon sources for yeast growth as a precondition of hydrogen peroxide induced hormetic phenotype. *Int. J. Microbiol.* **2015**, 1–8 (2015).
58. Kirchman, P. A. & Botta, G. Copper supplementation increases yeast life span under conditions requiring respiratory metabolism. *Mech Ageing Dev* **128**(2), 187–195 (2007).

59. Liang, Q. & Zhou, B. Copper and manganese induce yeast apoptosis via different pathways. *Mol Biol Cell* **18**(12), 4741–4749 (2007).
60. Nunez-Bajo, E. et al. Electrogeneration of gold nanoparticles on porous-carbon paper-based electrodes and application to inorganic arsenic analysis in white wines by chronoamperometric stripping. *Anal Chem* **89**(12), 6415–6423 (2017).
61. Guaragnella, N., et al. Signaling sustains mitochondrial respiratory capacity in HOG1-dependent osmoadaptation. *Microorganisms* **9**(9) (2021).
62. Di Noia, M. A., et al. Inactivation of HAP4 accelerates RTG-dependent osmoadaptation in *Saccharomyces cerevisiae*. *Int. J. Mol. Sci.* **24**(6) (2023).
63. Buscemi, G. et al. Bio-inspired redox-adhesive polydopamine matrix for intact bacteria biohybrid photoanodes. *ACS Appl Mater Interfaces* **14**(23), 26631–26641 (2022).
64. Ohsumi, Y., Kitamoto, K. & Anraku, Y. Changes induced in the permeability barrier of the yeast plasma membrane by cupric ion. *J Bacteriol* **170**(6), 2676–2682 (1988).
65. Azenha, M., Vasconcelos, M. T. & Moradas-Ferreira, P. The influence of Cu concentration on ethanolic fermentation by *Saccharomyces cerevisiae*. *J Biosci Bioeng* **90**(2), 163–167 (2000).
66. Mrvcic, J. et al. Optimization of bioprocess for production of copper-enriched biomass of industrially important microorganism *Saccharomyces cerevisiae*. *J Biosci Bioeng* **103**(4), 331–337 (2007).

Acknowledgements

E.W. and O.O. were recipients of PhD fellowships from the Italian Ministry of University and Research: Piano Stralcio «Ricerca e innovazione 2015-2017» del Fondo per lo Sviluppo e la Coesione. Anno Accademico 2020/2021—Ciclo XXXVI” [“Avviso D.D. 1233/2020”] for the projects “Biosensors development for precision agriculture” to N.G. and “BioSense-Biosensors for IoT-based Precision Farming” to C.G. This work was partially supported by the Nottingham Ningbo China Beacons of Excellence Research and Innovation Institute [budget code I01220800007].

Author contributions

Conceptualization: Enrico Marsili, Nicoletta Guaragnella, Ehtisham Wahid; Methodology: Enrico Marsili, Nicoletta Guaragnella, Matteo Grattieri; Investigation: Ehtisham Wahid, Sunday Olakunle Oguntomi, Run Pan, Ohiemi Benjamin Ocheja; Data curation: Ehtisham Wahid, Enrico Marsili, Sunday Olakunle Oguntomi; Writing—original draft: Ehtisham Wahid, Sunday Olakunle Oguntomi, Enrico Marsili, Nicoletta Guaragnella; Writing—review & editing: all authors.

Declarations

Competing interests

The authors have no conflict of interest to declare.

Additional information

Supplementary Information The online version contains supplementary material available at <https://doi.org/10.1038/s41598-025-86702-8>.

Correspondence and requests for materials should be addressed to E.M.

Reprints and permissions information is available at www.nature.com/reprints.

Publisher’s note Springer Nature remains neutral with regard to jurisdictional claims in published maps and institutional affiliations.

Open Access This article is licensed under a Creative Commons Attribution-NonCommercial-NoDerivatives 4.0 International License, which permits any non-commercial use, sharing, distribution and reproduction in any medium or format, as long as you give appropriate credit to the original author(s) and the source, provide a link to the Creative Commons licence, and indicate if you modified the licensed material. You do not have permission under this licence to share adapted material derived from this article or parts of it. The images or other third party material in this article are included in the article’s Creative Commons licence, unless indicated otherwise in a credit line to the material. If material is not included in the article’s Creative Commons licence and your intended use is not permitted by statutory regulation or exceeds the permitted use, you will need to obtain permission directly from the copyright holder. To view a copy of this licence, visit <http://creativecommons.org/licenses/by-nc-nd/4.0/>.

© The Author(s) 2025